Eur. Phys. J. B **39**, 513–519 (2004)
DOI: 10.1140/epjb/e2004-00224-8

THE EUROPEAN PHYSICAL JOURNAL B

Breakdown of universality in directed spiral percolation

S. Sinha and S.B. Santra[a]

Department of Physics, Indian Institute of Technology Guwahati, Guwahati-781039, Assam, India

Received 26 November 2003/ Received in final form 12 March 2004
Published online 23 July 2004 –

Abstract. Directed spiral percolation (DSP), percolation under both directional and rotational constraints, is studied on the triangular lattice in two dimensions ($2D$). The results are compared with that of the $2D$ square lattice. Clusters generated in this model are generally rarefied and have chiral dangling ends on both the square and triangular lattices. It is found that the clusters are more compact and less anisotropic on the triangular lattice than on the square lattice. The elongation of the clusters is in a different direction than the imposed directional constraint on both the lattices. The values of some of the critical exponents and fractal dimension are found considerably different on the two lattices. The DSP model then exhibits a breakdown of universality in $2D$ between the square and triangular lattices. The values of the critical exponents obtained for the triangular lattice are not only different from that of the square lattice but also different form other percolation models.

PACS. 02.50.-r Probability theory, stochastic processes, and statistics – 64.60.-i General studies of phase transitions – 72.80.Tm Composite materials

1 Introduction

A new site percolation model, directed spiral percolation (DSP), is recently introduced by Santra [1,2]. The DSP model is constructed imposing both directional and rotational constraints on the ordinary percolation (OP) model [3]. The directional constraint is in a fixed direction in space and the empty sites in that direction are accessible to occupation. Due to the rotational constraint the sites in the forward direction or in a rotational direction, say clockwise, are accessible to occupation. The direction of the rotational constraint is not fixed in space and it depends on the direction from which the present site is occupied. Percolation under only directional or only rotational constraints have been studied independently and the corresponding models are known as directed percolation (DP) [4] and spiral percolation (SP) [5] respectively. It is already known that both DP and SP models belong to different universality classes other than that of OP. The DSP model is essentially a combination of DP and SP models and it is constructed by imposing both the constraints simultaneously in the same model. Recently, the DSP model has been studied on the square lattice in 2 dimensions ($2D$) [1,2]. It has been found that a new type of percolation cluster is generated in this model. They are highly rarefied, anisotropic and chiral in nature. The elongation of the clusters is in a different direction from the imposed directional constraint. The values of the critical exponents obtained are different from that of the OP, DP and SP. Consequently, the DSP model belongs to a new universality class.

In this paper, the DSP model is studied on $2D$ triangular lattice and the results are compared with that of the square lattice data. The clusters are found more compact and less anisotropic on the triangular lattice than on the square lattice. Most interestingly, it is found that the values of the fractal dimension and some of the critical exponents of the DSP model are considerably different on the square and triangular lattices. Thus, there exists a breakdown of universality in the DSP model when the results of the square and triangular lattices are compared. In the following, the DSP model will be described briefly. The results of the triangular lattice will be then presented and compared with the square lattice data.

2 The model

Detailed description of the model on the square lattice is given in reference [1]. A brief demonstration will be given here on the triangular lattice. A left to right directional constraint and a clockwise rotational constraint are imposed on the system defined on a triangular lattice of size $L \times L$. Due to the directional constraint an empty site on the right of an occupied site and due to the rotational constraint the empty sites in the forward direction or in the clockwise direction can be occupied. To generate clusters under these two constraints a single cluster growth algorithm is developed in reference [1] following the original algorithm of Leath [6]. In this algorithm, the central

[a] e-mail: santra@iitg.ernet.in

site of the lattice is occupied with unit probability. All six nearest neighbours of the central site on the triangular lattice can be occupied with equal probability p in the first time step. As soon as a site is occupied, the direction from which it is occupied is assigned to it. Selection of empty nearest neighbour in the next MC time steps is illustrated in Figure 1. Two long arrows from left to right in Figure 1 represent the directional constraint. The presence of the rotational constraint is shown by the encircled dots. The black circles represent the occupied sites and the open circles represent the empty sites. The direction from which the central site is occupied is represented by a short thick arrow. Now the nearest neighbours of the central occupied site eligible for occupation will be identified. The dotted arrow indicates the eligible empty site for occupation due to the directional constraint and the thin arrows indicate the eligible empty sites for occupation due to the rotational constraint. Since the directional constraint is to the right, site 4 is always eligible for occupation. The rotational constraint acts in the forward or in the clockwise direction with respect to the direction of approach to the present occupied site. Since the central site is approached from 2, there are three sites, site 5 in the forward direction and sites 6 and 1 in the rotational direction, eligible for occupation due to rotational constraint. Note that, on the square lattice only two empty sites due to the rotational constraint were eligible for occupation at any MC step. It is also important to note that, in this model an occupied site can be reoccupied from a different direction due to the rotational constraint [1]. A site is forbidden for occupation from the same direction. On the triangular lattice, a site then could be occupied at most 6 times from 6 different directions. Due to the reoccupation of occupied sites, cluster generation is time consuming in the rotationally constrained models [7].

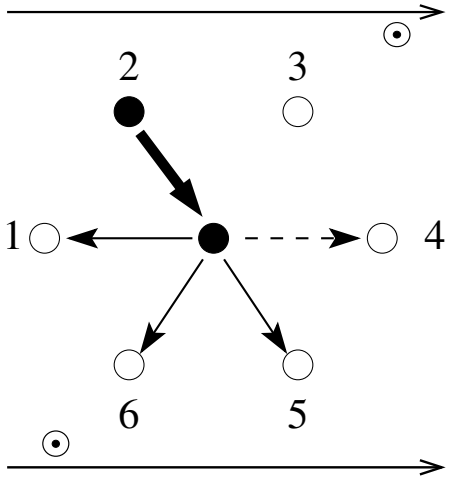

Fig. 1. Selection of eligible nearest neighbors for occupation of an already occupied site. Black circles are the occupied sites and open circles are the empty sites. Two thick long arrows from left to right represent the directional constraint. The presence of clockwise rotational constraint is shown by the encircled dots. The eligible nearest neighbors of the central occupied site will be selected here for occupation. Six nearest neighbours of the central site on the triangular lattice are marked as 1 to 6. The central site is occupied from the site 2, marked by a thick arrow. Due to directional constraint, site 4 on the right of the occupied site, is always eligible for occupation and it is indicated by a dotted arrow. Due to rotational constraint, sites 5, 6, and 1 are eligible for occupation and they are indicated by thin arrows.

After selecting the eligible sites for occupation, they are occupied with probability p. The coordinate of an occupied site in a cluster is denoted by (x,y). Periodic boundary conditions are applied in both directions and the coordinates of the occupied sites are adjusted accordingly whenever the boundary is crossed. At each time step the span of the cluster in the x and y directions $L_x = x_{max} - x_{min}$ and $L_y = y_{max} - y_{min}$ are determined. If L_x or $L_y \geq L$, the system size, then the cluster is considered to be a spanning cluster. The critical percolation probability p_c is defined as below which there is no spanning cluster and at $p = p_c$ a spanning cluster appears for the first time in the system.

3 Results and discussions

Simulations are performed on the triangular lattice of several different lattice sizes from $L = 128$ to $L = 2048$. The cluster size distribution $P_s(p)$ is defined as $P_s = N_s/N_{tot}$ where N_s is the number of s-sited finite clusters in a total of N_{tot} clusters generated. The percolation threshold p_c at which a spanning cluster appears for the first time in the system is determined by generating $N_{tot} = 5 \times 10^4$ clusters at different site occupation probability p. The probability to have a spanning cluster at a given site occupation probability p is given by $P_{sp} = n_{sp}/N_{tot} = 1 - \sum_s' P_s(p)$, where n_{sp} is the number of spanning clusters out of N_{tot} clusters. The percolation threshold p_c is determined from the maximum slope $(dP_{sp}/dp)_{max}$ of the curve P_{sp} versus p. In Figure 2, P_{sp} and dP_{sp}/dp are plotted against p for $L = 2048$. The percolation threshold p_c could be identified as $p_c = 0.5700 \pm 0.0005$ corresponding to the maximum slope. The derivative is calculated using the central difference method for the data points collected in an interval of 0.0005.

An infinite cluster generated on the triangular lattice of size $L = 256$ at $p_c = 0.5700$ is shown in Figure 3. The black dots are the occupied sites and the solid black circle on the upper left corner is the origin of the cluster. It could be seen that the elongation of the spanning cluster is almost along the left upper to the right lower diagonal of the lattice as it was seen on the square lattice. In the case of charged particles, this is due to the development of Hall voltage across the sample and perpendicular to the applied in-plane electric field. As a result, an effective directional field is developed along the left upper to the right lower diagonal of the lattice. It has already been observed on the square lattice that the DSP clusters are not merely the DP clusters in the presence of the effective field. The DSP clusters contain features other than the DP clusters. The

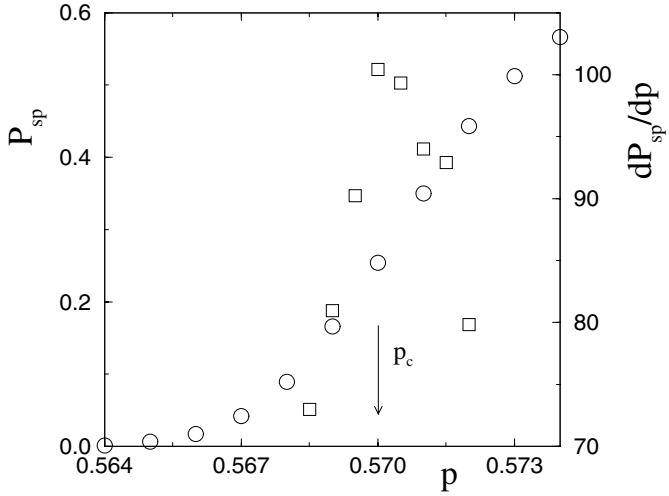

Fig. 2. Plot of spanning probability P_{sp} and the slope dP_{sp}/dp versus p. The circles represent P_{sp} and the squares represent the slope dP_{sp}/dp. The critical probability p_c is determined from the maximum slope. For the triangular lattice, it is found that $p_c = 0.5700 \pm 0.0005$ as indicated by an arrow.

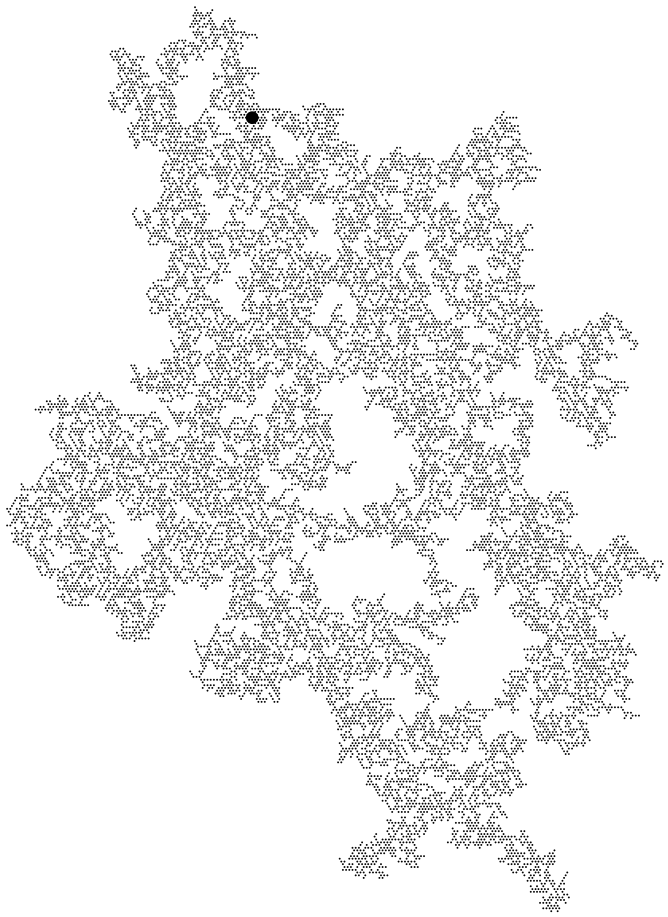

Fig. 3. An infinite cluster on a 256×256 triangular lattice at $p = 0.5700$ is shown. The black dots are the occupied sites. The solid black circle on the upper left corner is the origin of the cluster. The cluster has holes of almost all possible sizes. The elongation of the cluster is along the upper left to the lower right diagonal and not along the imposed directional constraint from left to right. The dangling ends are clockwisely rotated.

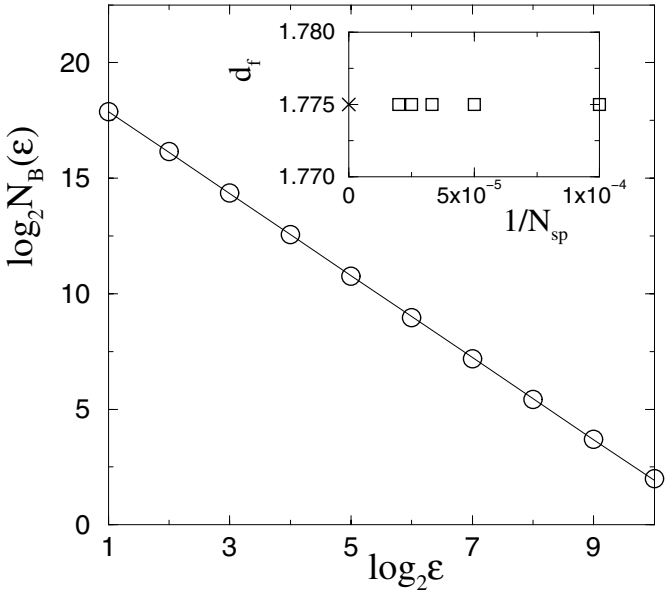

Fig. 4. Number of boxes $N_B(\epsilon)$ is plotted against the box size ϵ. Data are averaged over $50,000$ spanning clusters generated on a triangular lattice of size $L = 2048$. The fractal dimension is found $d_f = 1.775 \pm 0.004$. In the inset, d_f is plotted against $1/N_{sp}$, the number of spanning clusters. It could be seen that the value has converged with the realizations.

clusters here contain holes of almost all possible sizes and it has clockwisely rotated (chiral) dangling ends. It could also be noticed that the infinite cluster on the triangular lattice is more compact and less anisotropic in comparison to the infinite cluster on the square lattice.

The fractal dimension d_f of the infinite clusters at $p_c = 0.5700$ on the triangular lattice of size $L = 2048$ is determined by the box counting method. The number of boxes $N_B(\epsilon)$ is expected to grow with the box size ϵ as $N_B(\epsilon) \sim \epsilon^{d_f}$ where d_f is the fractal dimension. In Figure 4, $N_B(\epsilon)$ is plotted against the box size ϵ. The data are averaged over 5×10^4 spanning clusters. A reasonably good straight line is obtained in the $\log - \log$ scale. The fractal dimension is found $d_f = 1.775 \pm 0.004$. The error is due to the least square fitting of the data points taking into account the statistical error of each point. In order to check the convergence of the value of the fractal dimension, d_f is plotted against $1/N_{sp}$ in the inset of Figure 4. It could be seen that the value of d_f remains unchanged over 10^4 to 5×10^4 spanning clusters. The value of d_f has also been estimated from finite size (FS) scaling $S_\infty \sim L^{d_f}$, where S_∞ is the size of the largest cluster at $p = p_c$. The lattice size L changes from 2^7 to 2^{11}. It is found that $d_f(FS) = 1.80 \pm 0.03$, which is within the error bar of the other estimate. The fractal dimension d_f obtained here is higher than that of $d_f \approx 1.733$ [1] ($d_f(FS) \approx 1.72$ [2]) on the square lattice. Also notice that the value of d_f obtained here is smaller than the fractal dimensions obtained in OP (91/48 [8]) and SP (1.969 [9]) and it is slightly higher than DP (1.765 [7]). Vacancies are generated into the cluster as it grows. At the same time, due to the higher number of branching on the triangular

lattice the cluster penetrate into itself more and more than on the square lattice. As a result, the infinite clusters are less rarefied on the triangular lattice than on the square lattice.

Since the fractal dimension d_f is different from that of the square lattice value, it is then expected that the values of the other critical exponents will also be different form that of the square lattice in order to satisfy the scaling relations among the critical exponents. The critical exponents related to the different moments of the cluster size distribution $P_s(p)$ are now estimated. The scaling function form of the cluster size distribution $P_s(p)$ for single cluster growth technique, in which the central site is occupied with unit probability, is assumed to be

$$P_s(p) = s^{-\tau+1}\mathrm{f}[s^{\sigma}(p-p_c)] \qquad (1)$$

where τ and σ are two exponents. The assumed form of the scaling function $P_s(p)$ is the same as that of the square lattice. The first moment $\chi = \sum_s' sP_s(p)$ corresponds to the average cluster size. Next two higher moments are defined as $\chi_1 = \sum_s' s^2P_s(p)$ and $\chi_2 = \sum_s' s^3P_s(p)$. The primed sum represents the sum over all the finite clusters. As $p \to p_c$, the moments χ, χ_1, and χ_2 of $P_s(p)$ become singular with their respective critical exponent γ, δ, and η. The critical exponents are defined as

$$\chi \sim |p-p_c|^{-\gamma}, \;\; \chi_1 \sim |p-p_c|^{-\delta}, \;\; \& \;\; \chi_2 \sim |p-p_c|^{-\eta}. \qquad (2)$$

To estimate the values of γ, δ and η on the triangular lattice, the average cluster size χ and two other higher moments χ_1 and χ_2 are measured generating 5×10^4 finite clusters below p_c for different p values on several lattice sizes. In Figure 5, χ, χ_1 and χ_2 are plotted against $|p-p_c|$ for the system size $L = 2048$. The circles represent χ, the squares represent χ_1 and the triangles represent χ_2. The values of the exponents obtained are $\gamma = 1.98 \pm 0.01$, $\delta = 4.30 \pm 0.02$ and $\eta = 6.66 \pm 0.04$ for $L = 2048$. The errors quoted here are the standard least square fit error taking into account the statistical error of each single data point. Because of the error bar $\Delta p_c = 0.0005$ in the threshold, all the exponents have also been estimated for two other critical probabilities $p_c \pm \Delta p_c$. The values of the exponents obtained for $p = 0.5695$ are $\gamma \approx 1.96$, $\delta \approx 4.27$, and $\eta \approx 6.60$ whereas for $p = 0.5705$ they are $\gamma \approx 2.00$, $\delta \approx 4.33$ and $\eta \approx 6.71$. The values of the critical exponents are then taken as: $\gamma = 1.98 \pm 0.02$, $\delta = 4.30 \pm 0.04$ and $\eta = 6.66 \pm 0.08$. The values of the critical exponents at the optional thresholds $p_c \pm \Delta p_c$ are now within error bars. A comparison of the values of the critical exponents obtained on the triangular and square lattices is made in Figure 6 for several lattice sizes. In Figure 6, the values of γ, δ and η are plotted against the inverse system size $1/L$. The squares represent the square lattice data and the triangles represent the triangular lattice data. The data for the square lattice is taken from reference [1] except for $L = 2048$. In reference [1], data were reported upto the maximum lattice size $L = 1024$. For the sake of comparison with $L = 2048$ triangular lattice data, new estimates of the critical exponents have also been made on $L = 2048$

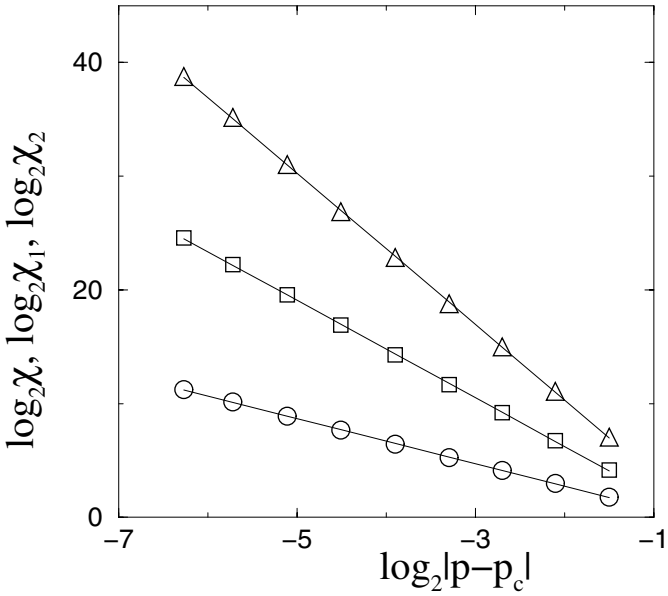

Fig. 5. Plot of the first, second and third moments χ, χ_1, and χ_2 of the cluster size distribution versus $|p-p_c|$ for a triangular lattice of size $L = 2048$. Different symbols are: circles for χ, squares for χ_1, and triangles for χ_2. The solid lines represent the best fitted straight lines through the data points. The corresponding critical exponents are found as $\gamma = 1.98 \pm 0.02$, $\delta = 4.30 \pm 0.04$, and $\eta = 6.66 \pm 0.08$.

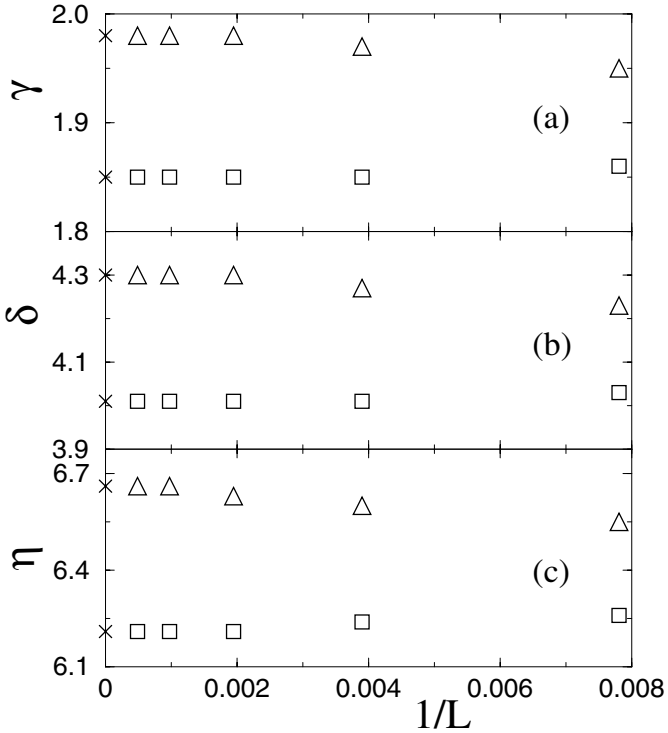

Fig. 6. Plot of the exponents γ, δ and η against the inverse system size $1/L$. The system sizes considered are: $L = 128, 256, 512, 1024$ and 2048. The squares represent the square lattice data and the triangles represent the triangular lattice data. The exponents are extrapolated upto $L \to \infty$ and the extrapolated values are marked by crosses. It can be seen that the exponents are significantly different on the two lattices.

square lattice. The results of $L = 2048$ square lattice are in good agreement with that of the smaller system sizes. On the square lattice of size $L = 2048$, the values of the critical exponent obtained are: $\gamma = 1.85 \pm 0.01$, $\delta = 4.01 \pm 0.04$ and $\eta = 6.21 \pm 0.08$. The results on both the lattices are then extrapolated upto $L \to \infty$, the infinite system size. The extrapolated values of the exponents are marked by crosses. The values of the critical exponents are found very different (beyond the error bars) on the square and triangular lattices. The triangular lattice values of the exponents are higher than that of the square lattice. The clusters then grow much larger in size on the triangular lattice than on the square lattice for a given p. This might be due to higher number of branching possibilities on the triangular lattice. Also notice that the value of $2\delta - \gamma = 6.62$ is very close to the value of the exponent $\eta = 6.66$. The values of the exponents then satisfy the scaling relation $\eta = 2\delta - \gamma$ [1] within error bars. The exponents are not only different from the square lattice values but also different from that of other percolation models, OP [1,8], DP [1,10] and SP [1,5,7].

There are two connectivity lengths, $\xi_\parallel$ and $\xi_\perp$, for the anisotropic clusters. Here, $\xi_\parallel$ is along the elongation of the cluster and $\xi_\perp$ is along the perpendicular direction to the elongation. The connectivity lengths are defined as $\xi_\parallel^2 = 2\sum_s' R_\parallel^2 sP_s(p)/\sum_s' sP_s(p)$ and $\xi_\perp^2 = 2\sum_s' R_\perp^2 sP_s(p)/\sum_s' sP_s(p)$ where $R_\parallel$ and $R_\perp$ are the radii of gyration with respect to two principal axes of the cluster. They are estimated from the eigenvalues of the moment of inertia tensor, a 2×2 matrix here. $\xi_\parallel$ and $\xi_\perp$ diverge with two different critical exponents $\nu_\parallel$ and $\nu_\perp$ as $p \to p_c$. The critical exponents $\nu_\parallel$ and $\nu_\perp$ are defined as

$$\xi_\parallel \sim |p - p_c|^{-\nu_\parallel} \quad \& \quad \xi_\perp \sim |p - p_c|^{-\nu_\perp}. \qquad (3)$$

The connectivity lengths, $\xi_\parallel$ and $\xi_\perp$, for the system size $L = 2048$ are plotted against $|p - p_c|$ in Figure 7. Data are averaged over 5×10^4 clusters. The squares represent $\xi_\parallel$ and the circles represent $\xi_\perp$. The corresponding exponents are $\nu_\parallel = 1.36 \pm 0.02$ and $\nu_\perp = 1.23 \pm 0.02$. The errors quoted here are the least square fit errors. The values of the exponents are also estimated at $p_c \pm \Delta p_c$. For $p = 0.5695$, the values obtained are $\nu_\parallel \approx 1.35$ and $\nu_\perp \approx 1.21$ and for $p = 0.5705$, the values obtained are $\nu_\parallel \approx 1.37$ and $\nu_\perp \approx 1.24$. There is a little variation and the values of the critical exponents are approximated as: $\nu_\parallel = 1.36 \pm 0.02$ and $\nu_\perp = 1.23 \pm 0.02$. The error bars now include the values of $\nu_\parallel$ and $\nu_\perp$ at the optional p_cs. To compare the square and triangular lattice data, simulations have been performed on other smaller system sizes. In Figure 8, the exponents $\nu_\parallel$ and $\nu_\perp$ are plotted against the inverse system sizes $1/L$ for both the square and triangular lattices. The squares represent the square lattice data and the triangles represent the triangular lattice data. Data of the square lattice is taken from reference [1] except for $L = 2048$. New estimates of the exponents are also made on $L = 2048$ square lattice. The exponents are extrapolated upto $L \to \infty$ and they are marked by crosses. Notice that, the exponent $\nu_\parallel$ is almost the same as that of the square lattice value (≈ 1.33) whereas $\nu_\perp$ is higher

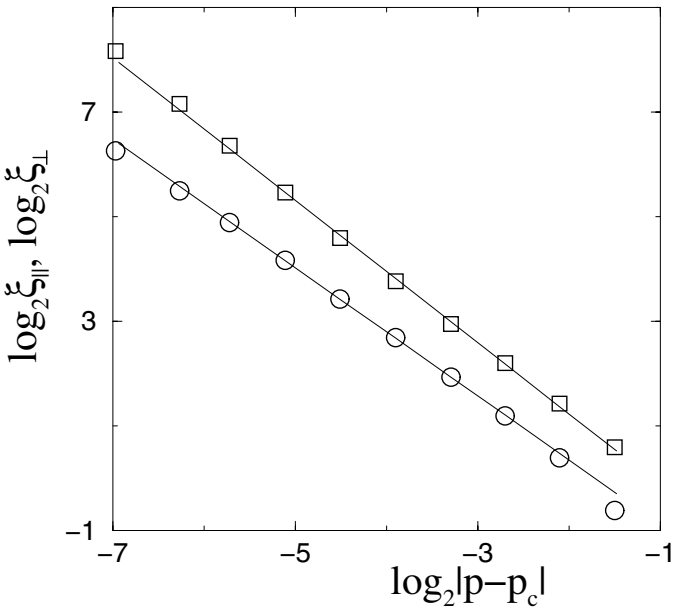

Fig. 7. The connectivity lengths, $\xi_\parallel$ and $\xi_\perp$, are plotted against $|p - p_c|$ for a triangular lattice of size $L = 2048$. The circles represent $\xi_\perp$ and the squares represent $\xi_\parallel$. The solid lines represent the best fitted lines through the data points. The critical exponents are found as $\nu_\parallel = 1.36 \pm 0.02$ and $\nu_\perp = 1.23 \pm 0.02$.

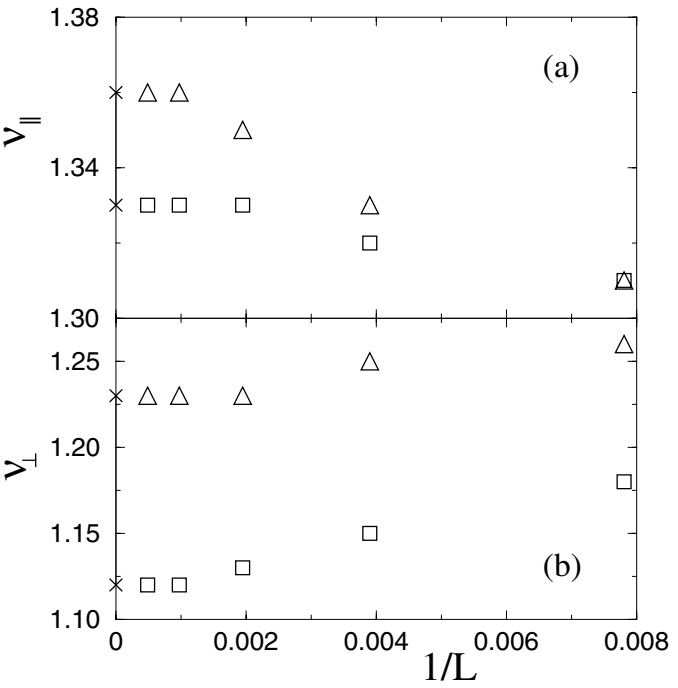

Fig. 8. The connectivity exponents $\nu_\parallel$ and $\nu_\perp$ are plotted against the inverse system size $1/L$ for the square and triangular lattices. The system size changes form $L = 128$ to 2048 as in Figure 6. The squares represent the square lattice data and the triangles represent the triangular lattice data. Extrapolated values to the infinite system size ($1/L = 0$) are marked by crosses. The value of $\nu_\perp$ seems to be different on the two lattices whereas $\nu_\parallel$ is close to the square lattice value.

Table 1. Comparison of the critical exponents and fractal dimension of the DSP model measured on the square and triangular lattices. For the square lattice, the values within parenthesis are the suggested rational fractions for the values of the critical exponents in reference [1] which satisfy the scaling relations exactly. Some of the critical exponents and the fractal dimension are significantly different on the two lattices.

Lattice Type	d_f	γ	δ	η	$\nu_\parallel$	$\nu_\perp$
Square [1]:	1.733 ± 0.005	1.85 ± 0.01	4.01 ± 0.04	6.21 ± 0.08	1.33 ± 0.01	1.12 ± 0.03
	(12/7)	(11/6)	(24/6)	(37/6)	(4/3)	(7/6)
	1.72 ± 0.02 (FS)					
Triangular:	1.775 ± 0.004	1.98 ± 0.02	4.30 ± 0.04	6.66 ± 0.08	1.36 ± 0.02	1.23 ± 0.02
	1.80 ± 0.03 (FS)					

than that of the square lattice ($\approx$ 1.12). Both the exponents are also different form that of DP model [1,10]. The hyperscaling relations $2\delta - 3\gamma = (d-1)\nu_\perp + \nu_\parallel$ and $(d - d_f)\nu_\perp = \beta = \delta - 2\gamma$ [1] are satisfied marginally: $2\delta - 3\gamma = 2.66 \pm 0.06$ whereas $(d-1)\nu_\perp + \nu_\parallel = 2.59 \pm 0.04$ and $\delta - 2\gamma = 0.34 \pm 0.06$ whereas $(d - d_f)\nu_\perp = 0.28 \pm 0.03$. It is already known that the hyperscaling is violated in directed percolation [11]. In the case of DSP, the hyperscaling relations were found satisfied on the square lattice whereas on the triangular lattice they are "marginally" satisfied. The ratio of the connectivity lengths goes as $\xi_\parallel/\xi_\perp \sim |p - p_c|^{-\Delta\nu}$ where $\Delta\nu = \nu_\parallel - \nu_\perp$. For the square lattice, $\Delta\nu$ is approximately 0.21 whereas for the triangular lattice, it is approximately 0.13. Thus, the clusters are less anisotropic on the triangular lattice. This is because of more flexibility given to the spiraling constraint which makes the cluster not only compact but also less anisotropic.

The values of the critical exponents and fractal dimension obtained in the above study for the triangular lattice are summarized and compared with the square lattice data in Table 1. The values in the parenthesis are the suggested rational fractions for the values of the critical exponents on the square lattice. These rational fractions satisfy the scaling relations exactly including the hyperscaling relations. It can be seen that some of the critical exponents and the fractal dimensions are considerably different on the square and triangular lattices for the DSP model. According to the theory of critical phenomena, the values of the critical exponents are independent of the underlaying lattice structure in the same spatial dimension. As a consequence, the systems defined on different lattices in the same space dimension then belong to the same universality class. Since the values of the critical exponents of the DSP model differ on the square and triangular lattices in $2D$, the DSP model then exhibits a breakdown of universality. This is the first percolation model which shows breakdown of universality on two different lattices in the same spatial dimension. It is already seen in the above discussion that the flexibility in the spiraling constraint makes the clusters compact and less anisotropic. A possible reason for different critical behaviour on the square and triangular lattices may be due to different scaling behaviour of the finite clusters below percolation threshold on the two lattices. Below p_c, the finite clusters are called lattice animals [12]. Lattice animals without any loop are known as lattice trees. Though the spiral lattice animals have the same scaling form on the square and triangular lattices, it has been found that the spiral trees (lattice animals without loops) follow two different scaling relations on the square and triangular lattices and belong to two different universality classes [13]. In the asymptotic $n \to \infty$ limit, the number of spiral lattice site trees (a_n) of n-sites on the triangular lattice obey the scaling relation given by $a_n \approx \lambda^{n^\delta} n^{-\theta}$ [13] whereas on the square lattice it is given by $a_n \approx \lambda^n n^{-\theta}$ [14], where δ and θ are two exponents and λ is known as the growth parameter. The origin of different scaling forms for the spiral lattice site trees on the square and triangular lattices is due to the fact that they can not have branching on the triangular lattice except at the origin whereas on the square lattice branching is possible at any point. The radius of gyration exponent of spiral trees was also found different on the square ($\nu \approx 0.653$) and triangular lattices ($\nu \approx 0.618$) [13]. Another lattice statistical model, the spiral self-avoiding walks (SAW) also exhibit breakdown of universality on the square and triangular lattices. The asymptotic (large n) behaviour of the number of walks S_n is given by $S_n \approx An^{-\gamma} \exp(\lambda\sqrt{n})$, where $A = 2^{-2} \times 3^{-5/4}\pi$, $\gamma = 7/4$, and $\lambda = 2\pi/\sqrt{3}$ for the square lattice [15] and $A = 2^{1/4} \times 3^{-7/4}\pi$, $\gamma = 5/4$, and $\lambda = \pi/\sqrt{2/3}$ for the triangular lattice [16]. Notice that the scaling relation for the spiral lattice site trees is similar to that of the spiral SAWs. It should be mentioned here that the values of the critical exponents and the scaling behaviour of the cluster related quantities in the SP model (percolation in the presence of rotational constraint only) are the same on the square and triangular lattices and no breakdown of universality has been observed [7]. This may be due to the fact that the spiral lattice trees are minority in number at the percolation threshold and unable to change the universality class. In the DSP model, the presence of the directional constraint on top of the rotational constraint might increase the number of spiral lattice trees. Maybe, the higher number of tree like structures in the clusters generated has a non-trivial effect on the critical properties of the DSP model at the percolation threshold and leads to breakdown of universality of the critical exponents.

Finally, the form of the scaling function $P_s(p) = s^{-\tau+1}\mathrm{f}[s^\sigma(p - p_c)]$ is verified. The exponents τ and σ are estimated using the scaling relations $\beta = (\tau - 2)/\sigma$,

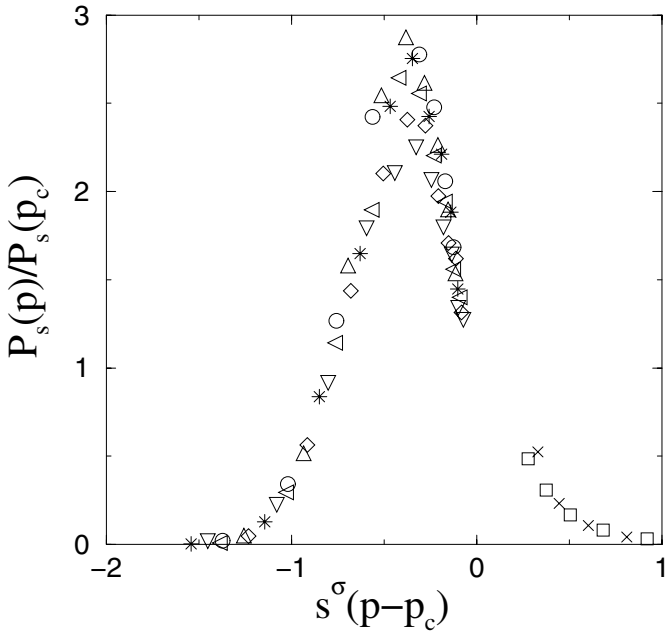

Fig. 9. Plot of the scaled cluster size distribution $P_s(p)/P_s(p_c)$ versus the scaled variable $s^\sigma(p-p_c)$ for different values of p on the triangular lattice. The value of σ is taken as $\sigma = 0.427$. The cluster size s changes from 64 to 16384. The data plotted correspond to $p - p_c = 0.007(\times)$, $0.005(\square)$, $-0.035(\triangledown)$, $-0.04(\Diamond)$, $-0.045(\triangleleft)$, $-0.05(*)$, $-0.055(\triangle)$, $-0.06(\bigcirc)$. A reasonable data collapse is observed.

$\gamma = (3-\tau)/\sigma$, $\delta = (4-\tau)/\sigma$, and $\eta = (5-\tau)/\sigma$ and following the same technique described in reference [1]. The estimates of τ and σ are obtained as $\tau = 2.16 \pm 0.02$ and $\sigma = 0.427 \pm 0.003$ respectively. The errors quoted here are the propagation errors. On the square lattice, the values of τ and σ were obtained as ≈ 2.16 and 0.459 respectively. Note that, the value of τ is the same as that of the square lattice whereas σ differs on the two lattices. The scaling function form is verified through data collapse by plotting $P_s(p)/P_s(p_c)$ against the scaled variable $s^\sigma(p-p_c)$ in Figure 9. The cluster size s changes from 64 to 16384 and $(p-p_c)$ varies from 0.007 to -0.06. A reasonable data collapse is observed. The scaling function form is similar to that of the square lattice. The height of the function remains almost the same but the width is slightly smaller than that of the square lattice function. The lesser width of the scaling function $P_s(p)$ is just a consequence of the lesser value of σ on the triangular lattice.

4 Conclusion

The directed spiral site percolation is studied on the triangular lattice and the results are compared with that of the square lattice. Clusters on the triangular lattice are found more compact and less anisotropic than the clusters on the square lattice. Interestingly, it is also found that the values of the fractal dimension and some of the critical exponents on the triangular lattice are significantly different from the square lattice values. This might be due to different scaling behaviour of some of the finite clusters below percolation threshold on the two lattices. As a consequence, the DSP model exhibits a breakdown of universality between the square and triangular lattices in $2D$. The values of the critical exponents on both the lattices satisfy the scaling relations between the moment exponents (γ, δ, η). The hyperscaling relations were satisfied on the square lattice but they are "marginally" satisfied on the triangular lattice. The exponents are not only different on the square and triangular lattices but also different from other percolation models like OP, DP and SP. Directed spiral percolation is expected to occur in disordered systems when both rotational and directional force fields are present.

The authors thank Deepak Dhar for helpful discussions. SS thanks CSIR, India for financial support.

References

1. S.B. Santra, Eur. Phys. J. B **33**, 75 (2003)
2. S.B. Santra, Int. J. Mod. Phys. B **17**, 5555 (2003)
3. D. Stauffer, A. Aharony, *Introduction to Percolation Theory*, 2nd edn. (Taylor and Francis, London, 1994); A. Bunde, S. Havlin, in *Fractals and Disordered Systems*, edited by A. Bunde, S. Havlin (Springer-Verlag, Berlin, 1991)
4. W. Kinzel, in *Percolation Structure and Processes*, edited by G. Deutscher, R. Zallen, J. Adler (Adam Hilger, Bristol, 1983); H. Hinrichsen, Adv. Phys. **49**, 815 (2000)
5. P. Ray, I. Bose, J. Phys. A **21**, 555 (1988); S.B. Santra, I. Bose, J. Phys. A **24**, 2367 (1991)
6. P.L. Leath, Phys Rev. B **14**, 5046 (1976)
7. S.B. Santra, I. Bose, J. Phys. A **25**, 1105 (1992)
8. M.P.M. den Nijs, J. Phys. A **12**, 1857 (1997); B. Nienhuis, J. Phys. A **15**, 199 (1982)
9. B. Hede, J. Kertész, T. Vicsek, J. Stat. Phys. **64**, 829 (1991)
10. J.W. Essam, K. DéBell, J. Adler, Phys. Rev. B **33**, 1982 (1986); J.W. Essam, A.J. Guttmann, K. DéBell, J. Phys. A **21**, 3815 (1988)
11. M. Henkel, V. Privman, Phys. Rev. Lett. **65**, 1777 (1990)
12. T.C. Lubensky, J. Isaacson, Phys. Rev. Lett. **46**, 871 (1981)
13. S.B. Santra, J. Phys. I France **5**, 1573 (1995)
14. I. Bose, P. Ray Phys. Rev. B **35**, 2071 (1987); I. Bose, P. Ray, D. Dhar, J. Phys. A **21**, L219 (1988); I. Bose, P. Ray, S. Mukhopadhyay, J. Phys. A **21**, L979 (1988); S.B. Santra, I. Bose, J. Phys. A **22**, 5043 (1989)
15. H.J.W. Blöte, H.J. Hilhorst, J. Phys. A **17**, L111 (1984)
16. K.Y. Lin, J. Phys. A **18**, L145 (1985)